Defense Technical Information Center
Compilation Part Notice

ADP012061

TITLE: Methods for the Evaluation of Regular, Weakly Singular and Strongly Singular Surface Reaction Integrals Arising in Method of Moments

DISTRIBUTION: Approved for public release, distribution unlimited

This paper is part of the following report:

TITLE: Applied Computational Electromagnetics Society Journal. Volume 17, Number 1

To order the complete compilation report, use: ADA399939

The component part is provided here to allow users access to individually authored sections of proceedings, annals, symposia, etc. However, the component should be considered within the context of the overall compilation report and not as a stand-alone technical report.

The following component part numbers comprise the compilation report:
ADP012055 thru ADP012066

Methods for the Evaluation of Regular, Weakly Singular and Strongly Singular Surface Reaction Integrals Arising in Method of Moments

Alexander Herschlein, Jürgen v. Hagen, *Member ACES*, Werner Wiesbeck

Institut für Höchstfrequenztechnik und Elektronik, Universität Karlsruhe
Kaiserstr. 12, D - 76128 Karlsruhe
Tel: +49 721 608 76 76, Fax: +49 721 69 18 65, Email vonhagen@ihe.etec.uni-karlsruhe.de

Abstract - The accurate and fast evaluation of surface reaction integrals for Method of Moments computations is presented. Starting at the classification of the integrals into regular and weakly, strongly and nearly singular integrals, appropriate methods are presented that handle each. A Gauss-Legendre quadrature rule evaluates regular integrals. For singular integrals, the singularity is lifted or weakened by an extraction of the singularity, a transform to polar coordinates or a domain transform. The resulting regular integral is in turn solved by a quadrature rule. The different methods are finally applied to an example, and the resulting accuracy tested against the analytical result. The presented methods are general enough to be used as integration methods for integrands with various degrees of singularity and is not limited to Method of Moments.

1.   INTRODUCTION

The solution of integro-differential equations by the Method of Moments is directly influenced by the accuracy of the matrix elements corresponding to the reaction integrals. Efficient and accurate methods for the evaluation of the reaction integrals are hence necessary. The numerical methods must fulfill two major requirements. First, the method should converge quickly to ensure a low computation time. Second, the evaluation should be accurate in order to obtain a good overall accuracy.

The evaluation of the reaction integrals gives rise to integrals whose kernel include the free-space Green's function and its derivatives [PM73]. This necessitates the proper treating of four kinds of integrands. First, regular integrals are solved by usual quadrature rules. Second, weakly singular integrands require mathematical transforms before integrating. Third, strongly singular integrands are only accesible to specialized integration methods. Finally, observation points that are located very close to the integrational domain give rise to nearly singular integrals. This paper presents powerful integration methods for each integral.

The first purpose of the paper is to present different methods and their applicability to the different types of integrals. The second purpose is to present a new accurate method to evaluate strongly singular kernels. The third purpose is to carefully compare the appropriate integration methods. To the authors' knowledge, the present complete description of the integration methods is not available in the literature as such.

The organization of the paper is as follows. The following section presents the classification of the kernels. Then, the four methods for regular, nearly singular, weakly singular and strongly singular integrands are presented with an example of a rectangular surface element [HvHW00]. A comparison of the methods closes the presentation.

2.   KERNEL CLASSIFICATION

The reaction integrals within a Method of Moments computation involve the integration of the Green's functions or their derivative together with the basis functions and testing functions [PM73].

The free-space Green's function with a source point at r' $G(\vec{r},\vec{r}') = e^{-j\beta|\vec{r}-\vec{r}'|}/\left(4\pi|\vec{r}-\vec{r}'|\right)$ and its derivative $\nabla G(\vec{r},\vec{r}')$ $= -\nabla'G(\vec{r},\vec{r}')$ determine the behavior of the kernels. The distance factor R contained in the Green's function is:

$$R = |\vec{r}-\vec{r}'| = \sqrt{\left(x^P - x'\right)^2 + \left(y^P - y'\right)^2 + \left(z^P - z'\right)^2} \qquad (1)$$

and determines if the integrand at the point P is regular (for $\vec{r} \neq \vec{r}'$) or singular (for $\vec{r} = \vec{r}'$).

For the following, the propagation constant β is separated into a real and an imaginary part:

$$\beta = \omega\sqrt{\mu_0\left(\varepsilon' - j\varepsilon'' - j\kappa/\omega\right)} = \beta' + j\beta'' \qquad (2)$$

with the usual material parameters ε, μ and κ and the angular frequency ω.

One obtains then:

$$G = \frac{e^{-j\beta R}}{4\pi R} = \frac{e^{\beta''R}}{4\pi R}\left(\cos\left(\beta'R\right) - j\sin\left(\beta'R\right)\right) \qquad (3)$$

The derivative $\nabla'G(\vec{r},\vec{r}')$ in cartesian coordinates is then:

$$\begin{aligned}
\nabla'G = {} & \frac{\vec{r}'-\vec{r}}{R^3}\frac{e^{\beta''R}}{4\pi}\left[-\cos\left(\beta'R\right) + j\sin\left(\beta'R\right)\right] \\
& + \frac{\vec{r}'-\vec{r}}{R^2}\frac{e^{\beta''R}}{4\pi}\left[-\beta'\sin\left(\beta'R\right) + \beta''\cos\left(\beta'R\right)\right. \\
& \left. - j\left(\beta'\cos\left(\beta'R\right) + \beta''\sin\left(\beta'R\right)\right)\right]
\end{aligned} \qquad (4)$$

Consider each term in (3) and (4) when the observation point P moves closer to the source point, or $R \to 0$. In this case, (3) and (4) become singular, the order of their singularity is listed in Table 1. The imaginary part (5) of the Green's function is regular, and further, the derivative of the Green's function has a regular term (6). Mathematically, (5) and (6) can be integrated with no further problems.

The real part of the Green's function (7) and parts (8) of the derivative of the Green's function are weakly singular with terms $\sim 1/R$. This singularity can be easily regularized.

The last term (9) caused by the derivation of the Green's function is strongly singular $\sim 1/R^2$ for $R \to 0$. A regularisation must be carried out before an integration can be carried out. For the strongly singular case, the regularisation is more complicated than for the weakly singular case. Appropriate integration methods are necessary.

3. Integration Methods

The integration methods for the kernels in Table 1 are chosen according to the following three cases:

- $R > d$: the distance between the observation point P and the source point is greater than a predetermined minimal distance d (regular),
- $R < d$: the distance between the observation point P and the source point is smaller than a predetermined minimal distance d (regular, but nearly singular),
- $R \to 0$: observation point and source point P coincide (weakly and strongly singular).

Table 2 shows a summary of which integration method is applicable for the various source-observation point distances. As seen, special integration methods are needed that correctly treat regular, nearly singular, weakly singular and strongly singular integral kernels. They are in detail:
- *Regular integration:* Solved by a Gauss-Legendre quadrature method. The method is numerically accurate and easy to implement. Section 3.1 sketches the method.
- *Nearly singular integration:* For a distance R smaller than a minimal distance d, the integrand changes rapidly and becomes nearly singular. The appropriate integration method is laid out in section 3.4.
- *Weakly singular integration:* The method for weakly singular kernels is outlined in section 3.2. The integration involves either a domain transform, a transform to polar coordinates or an extraction of the singularity.

Table 1 Classification of the integrands for $R \to 0$

regular kernels	
$-\dfrac{e^{\beta''R}}{4\pi R} j \sin(\beta'R)$	(5)
$\dfrac{\vec{r}' - \vec{r}}{R^2} \dfrac{e^{\beta''R}}{4\pi} \left[-\beta' \sin(\beta'R) - j\beta'' \sin(\beta'R) \right]$	(6)

weakly singular kernels	$\sim 1/R$
$\dfrac{e^{\beta''R}}{4\pi R} \cos(\beta'R)$	(7)
$\dfrac{\vec{r}' - \vec{r}}{R^2} \dfrac{e^{\beta''R}}{4\pi} \left[\beta'' \cos(\beta'R) - j\left(\beta' \cos(\beta'R) - \dfrac{\sin(\beta'R)}{R} \right) \right]$	(8)

strongly singular kernels	$\sim 1/R^2$
$-\dfrac{\vec{r}' - \vec{r}}{R^3} \dfrac{e^{\beta''R}}{4\pi} \cos(\beta'R)$	(9)

Table 2 Integration methods for the various source-observation point distances R

regular kernels		
$\left.\begin{array}{l}R > d \\ R < d \\ R \to 0\end{array}\right\}$	regular integration	$\to$ section 3.1

weakly singular kernels		
$R > d$: regular integration		$\to$ section 3.1
$R < d$: nearly singular integration		$\to$ section 3.4
$R \to 0$: weakly singular integration		$\to$ section 3.2

singular kernels		
$R > d$: regular integration		$\to$ section 3.1
$R < d$: nearly singular integration		$\to$ section 3.4
$R \to 0$: strongly singular integration		$\to$ section 3.3

- *Strongly singular integration:* Two methods in section 3.3 carry out the integration of strongly singular kernels. The methods are composed of the methods for weakly singular and regular kernels. Section 3.3.2 presents a new method that combines the domain transform and the extraction of singularity. Transforms and an extraction of singularity regularize the singularities, the resulting kernels are integrated by the Gauss-Legendre quadrature as in 3.1.

3.1 Regular Integration

A direct Gauss-Legendre quadrature is proposed for the regular parts in Table 2 [Abr70], [Sch93]. In (10), the general Gauss-Legendre quadrature for a general, regular integrand $F(u_1,u_2)$ is given as:

$$\iint_{u_1,u_2} F(u_1,u_2)\sqrt{g(u_1,u_2)}du_1du_2$$

$$\sim \sum_{i=1}^{n_i}\sum_{j=1}^{n_j} F(u_i,u_j)\sqrt{g(u_i,u_j)}w_iw_j \tag{10}$$

F is a function of two continuous variables u_1 and u_2. They correspond to the surface variables on a surface element in the Method of Moments [HvHW00]. The expression $\sqrt{g(u_1,u_2)}du_1du_2$ is the differential surface element that expresses the transform of the surface differential into the u_1,u_2 system.

For the numerical integration, the u_i, u_j are the nodes on the surface in the interval $u_{1,2}=[-1,+1]$. The w_i and w_j are the weights for the nodes. Both are listed in the mathematical literature [Abr70] and are not repeated here.

3.2 Weakly Singular Integration

Three different methods are proposed in this section for the numerical computation of weakly singular kernels if $R\to 0$:

- section 3.2.1: regularization of the kernel by a transform into polar coordinates
- section 3.2.2: regularization by a domain transform
- section 3.2.3: regularization by an extraction of the singularity and subsequent analytical integration

All three integration methods are presented for the sake of completeness. The methods are later also used for the integration of strongly singular kernels.

As an example consider the weakly singular term $(x'-x^p)/(4\pi R^2)\beta'\cos(\beta'R)$ (8) on a planar rectangular element as in Fig. 1 with a size of $\lambda/10$ which is typical for a surface element in a Method of Moments implementation.
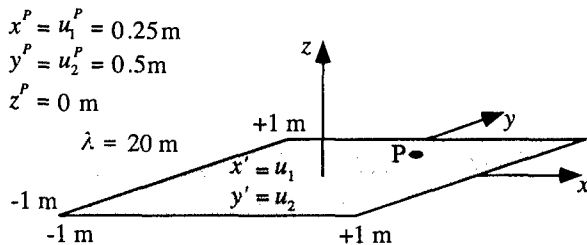
$$x^P = u_1^P = 0.25\,\text{m}$$
$$y^P = u_2^P = 0.5\,\text{m}$$
$$z^P = 0\,\text{m}$$
$$\lambda = 20\,\text{m}$$

Figure 1 Example geometry to outline integration accuracy.

3.2.1 Transform to Polar Coordinates

The singular point P is arbitrarily located on the surface element, with its normalized coordinates $u_1 = [-1,1]$, $u_2 = [-1,1]$. The weakly singular integrands are regularized by a transform into polar coordinates [GG90]. The process of regularization is depicted in Fig. 2. First, the surface element is partitioned into four rectangles V_k with the singular point P located on the corner that is common to all rectangles. Each rectangle is then in turn subdivided into two triangles, the integration is carried out on each of the eight triangles separately.
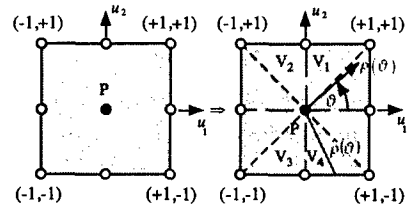
Figure 2 Sub-division of a discretization element into four quadrangles V_k and subsequent transform to polar coordinates.

The transform into polar coordinates ρ, ϑ is

$$u_1 = u_1^P + \rho\cos\vartheta \tag{11}$$
$$u_2 = u_2^P + \rho\sin\vartheta \tag{12}$$
$$du_1du_2 = \rho\, d\rho\, d\vartheta \tag{13}$$

The integral is then in polar coordinates

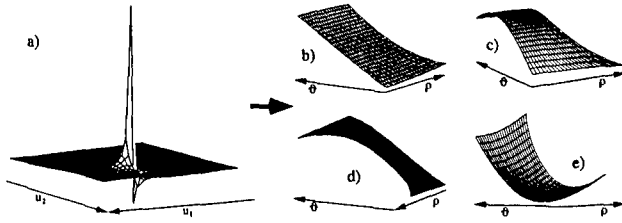$$\int_{-1}^{+1}\int_{-1}^{+1} F(u_1,u_2)\sqrt{g(u_1,u_2)}du_1du_2$$

$$= \sum_{k=1}^{4}\iint_{\rho,\vartheta} F_k(\vartheta,\rho(\vartheta))\sqrt{g_k(\vartheta,\rho(\vartheta))}\rho\, d\rho\, d\vartheta \tag{14}$$

The weight ρ that arises due to the transform from the u_1,u_2-system into the ρ,ϑ-system lifts the singularity and regularizes the integrand. The numerical integration of (14) is carried out by observing that the upper limit $\rho(\vartheta)$ is a function of ϑ.

For the above example, the regularization of the integrand is shown in Fig. 3. Fig 3a) shows the weakly singular integrand in the u_1,u_2-system. Fig 3b) to 3e) depict the regularized integrand in polar coordinates. The angle ϑ is defined on the following intervals for the triangles in 3.2.2:

- Fig. 3b): $4{,}02 \le \vartheta < 5{,}18$ and $\rho(\vartheta) = -1{,}5/\sin(\vartheta)$,
- Fig. 3c): $-1{,}1 \le \vartheta < 0{,}59$ and $\rho(\vartheta) = 0{,}75/\cos(\vartheta)$,
- Fig. 3d): $0{,}59 \le \vartheta < 2{,}76$ and $\rho(\vartheta) = 0{,}5/\sin(\vartheta)$,
- Fig. 3e): $2{,}76 \le \vartheta < 4{,}02$ and $\rho(\vartheta) = -1{,}25/\cos(\vartheta)$.
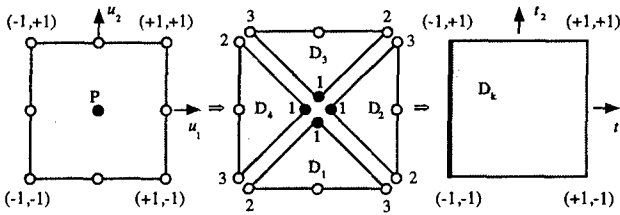
Figure 3 Transform of a weakly singular integrand into regular sub-integrands using a transform into polar coordinates. Each integrand is then normalized.

As seen in Fig. 3 b) to e), the integrands present a smooth behavior.

3.2.2   Domain Transform

Alternatively to the previous transform, the following domain transform may be used. First, the rectangle in the u_1,u_2 -system is subdivided (cf. Fig. 4) into the triangles D_1, D_2, D_3 and D_4 [Duf82, Dom93]. The singular point P is then located on the corner that is common to all triangles.

Figure 4 Subdivision of a surface element into triangles, and subsequent transform of a sub-triangle D_k into a rectangle.

A non-linear domain transform maps each triangle into a rectangle, the singular point P is mapped to a singular edge. The original variables u_1,u_2 are transformed to new surface variables $s_1 = [0,1]$ and $s_2 = [0,1]$ by:

$$u_1 = (1-s_1)u_1^{D_{k,1}} + s_1(1-s_2)u_1^{D_{k,2}} + s_1 s_2 u_1^{D_{k,3}}$$ (15)

$$u_2 = (1-s_1)u_2^{D_{k,1}} + s_1(1-s_2)u_2^{D_{k,2}} + s_1 s_2 u_2^{D_{k,3}}$$ (16)

The subscripts in the $D_{k,j}$ correspond to the number of each triangle $k = 1....4$ and its corner $i = 1....3$. Now, the interval is shifted to obtain symmetric integration limits

$$s_1 = (t_1 + 1)/2$$ (17)

$$s_2 = (t_2 + 1)/2$$ (18)

t_1 and t_2 are now from -1 to +1. The differentials are transformed by the Jacobian:

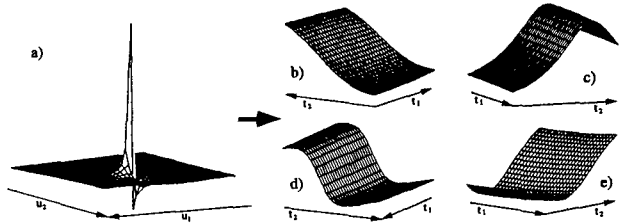$$du_1 du_2 = 2A^{D_k} ds_1 ds_2 = \frac{(t_1+1)A^{D_k}}{4} dt_1 dt_2$$ (19)

A^{D_k} are the surfaces of the triangles in the u_1,u_2-system. For source and observation points that are not in the centre $u_1 = 0$, $u_2 = 0$ of a surface element, the A^{D_k} are different for each triangle.

A weakly singular integral is hence regularized using the integration in (20):

$$\int_{-1}^{+1}\int_{-1}^{+1} F(u_1,u_2)\sqrt{g(u_1,u_2)}du_1 du_2$$

$$= \sum_{k=1}^{4}\int_{-1}^{+1}\int_{-1}^{+1} F_k(t_1,t_2)\sqrt{g_k(t_1,t_2)}\frac{(t_1+1)A^{D_k}}{4}dt_1 dt_2$$ (20)

The $\sqrt{g(u_1,u_2)}$ are the weights arising by the transform of the surface differential into the u_1,u_2-system. The transform of the differentials from the u_1,u_2-system into t_1,t_2-system is according to (19) adds the term (t_1+1) that lifts the singularity and regularizes the integrand.

In Fig. 5, the triangles arising in the regularization are depicted. 5b) to 5e) show the regularized integrands in the t_1,t_2-system. Again the integrands are very smooth.

Figure 5 Transform of a weakly singular integrand into regular sub-integrands using a domain transform The sub-integrands are normalized.

3.2.3   Singularity Extraction

The singularity of the Green's function can be lifted by subtracting an analytically integrable part. The method extracts the singularity in such a way that the extracted term is analytically integrated as in (21) for a singular point P:

$$\iint_{u_1,u_2}\frac{e^{-j\beta R}}{R}du_1 du_2 = \iint_{u_1,u_2}\left(\frac{e^{-j\beta R}}{R}-\frac{1}{R}\right)du_1 du_2 + \iint_{u_1,u_2}\frac{1}{R}du_1 du_2$$ (21)

By subtracting the inverse distance, the first integrand in (21) becomes regular. This term is integrated using the usual Gauss-Legendre integration as in section 3.1. The remaining singular integral in $1/R$ is integrated analytically.

For a linear triangular surface patch, the integration of $1/R$ can be carried out analytically with no approximation. For higher order geometrical surface approximation functions such as the biquadratic [HvHW00], however, the integration cannot be carried out analytically. In this case the integrand is developped into a series. For the x-coordinate, one obtains:

$$\left(x'-x^P\right) \approx \frac{\partial x'}{\partial u_1}\bigg|_{\substack{u_1=u_1^P\\u_2=u_2^P}}\left(u_1-u_1^P\right) + \frac{\partial x'}{\partial u_2}\bigg|_{\substack{u_1=u_1^P\\u_2=u_2^P}}\left(u_2-u_2^P\right) \tag{22}$$

y and z are analogous. Completing and combining the expressions in $x, y,$ and z leads to :

$$\frac{1}{R} \approx 1 \Big/ \sqrt{\begin{array}{l} g_{11}\big|_{\substack{u_1=u_1^P\\u_2=u_2^P}}\left(u_1-u_1^P\right)^2 + \\[2mm] g_{22}\big|_{\substack{u_1=u_1^P\\u_2=u_2^P}}\left(u_2-u_2^P\right)^2 + \\[2mm] 2g_{12}\big|_{\substack{u_1=u_1^P\\u_2=u_2^P}}\left(u_1-u_1^P\right)\left(u_2-u_2^P\right) \end{array}} \tag{23}$$

The integration according to u_1, u_2 in (23) is carried out analytically [SC95]. With the Taylor series, one finally obtains:

$$\begin{aligned} \iint_{u_{1a},u_{2a}}^{u_{1b},u_{2b}} & \frac{1}{R}du_1du_2 \\ & \approx \left[\frac{\left(u_1-u_1^P\right)}{\sqrt{g_{22}}}\ln\left[R+\sqrt{g_{22}}\left(u_2-u_2^P\right)+\frac{g_{12}}{\sqrt{g_{22}}}\left(u_1-u_1^P\right)\right]\right. \\ & \left.+\frac{\left(u_2-u_2^P\right)}{\sqrt{g_{11}}}\ln\left[R+\sqrt{g_{11}}\left(u_1-u_1^P\right)+\frac{g_{12}}{\sqrt{g_{11}}}\left(u_2-u_2^P\right)\right]\right]\bigg|_{u_1=u_{1a}}^{u_1=u_{1b}}\bigg|_{u_2=u_{2a}}^{u_2=u_{2b}} \end{aligned} \tag{24}$$

3.3 Strongly Singular Integration

For the integration of strongly singular integrands, the methods of section 3.2 are combined. The combinations yield regular integrands that are dealt with the method described in 3.1.

Two methods lift the singularity:
- The application of a transform to polar coordinates [PG89], [GG90], [GC87] and subsequent extraction of the singularity. This is presented in section 3.3.1.
- A new method in section 3.3.2 combines the domain transform and a subsequent extraction of the singularity. This new method yields very smooth integrands that are accessible to numerical integrations.

As an example, consider the integration of the singular kernel (9) in the geometry in Fig. 1.

3.3.1 Transform to Polar Coordinates and Extraction of Singularity

The transform to polar coordinates, origin at the point P, analogous to section 3.2.1, (11) and (12), $u_1 = u_1^P + \rho\cos\vartheta$, and $u_2 = u_2^P + \rho\sin\vartheta$, reduces the order of the singularity in (9) by one by virtue of the integration weight $du_1du_2 = \rho d\rho d\vartheta$. The resulting singularity is only weak, and the method for the extraction of the singularity in section 3.2.3 is applicable. The term that determines the singularity in (9) is given by:

$$\left(x'-x^P\right)\big/\left(4\pi R^3\right) \tag{25}$$

For an analytical integration in ρ, the integrand is developed into a series around the point P. With (11) and (12), $u_1-u_1^P = \rho\cos\vartheta$, $u_2-u_2^P = \rho\sin\vartheta$, one obtains for an x-component in (22):

$$\begin{aligned} \left(x'-x^P\right) &= \rho\left[\frac{\partial x'}{\partial u_1}\bigg|_{\substack{u_1=u_1^P\\u_2=u_2^P}}\cos\vartheta + \frac{\partial x'}{\partial u_2}\bigg|_{\substack{u_1=u_1^P\\u_2=u_2^P}}\sin\vartheta\right] + O(\rho^2) \\ &= \rho A_1(\vartheta) + O(\rho^2) \end{aligned} \tag{26}$$

Analogous to (26), the expressions for the y- and z-components yield expressions in $A_2(\vartheta)$ and $A_3(\vartheta)$. With these, one obtains the term that is necessary to express the distance R:

$$A(\vartheta) = \sqrt{A_1(\vartheta)^2 + A_2(\vartheta)^2 + A_3(\vartheta)^2} \tag{27}$$

The distance R depends now on polar coordinates and is given with (26) and (27):

$$R^2(\rho,\vartheta) = \rho^2 A^2(\vartheta) + O(\rho^3) \tag{28}$$

With (28) and $\left(x'-x^P\right)/R = A_1(\vartheta)/A(\vartheta) + O(\rho)$ one obtains:

$$\begin{aligned} \frac{\left(x'-x^P\right)}{R^3} &= \left(\frac{A_1(\vartheta)}{A(\vartheta)}+O(\rho)\right)\frac{1}{\rho^2 A^2(\vartheta)+O(\rho^3)} \\ &= \frac{1}{\rho^2}\left(\frac{A_1(\vartheta)}{A^3(\vartheta)}+\frac{O(\rho)}{A^2(\vartheta)+O(\rho)}\right) \end{aligned} \tag{29}$$

Incorporating the integration weight ρ for the transform of the differentials from the u_1,u_2-system into the ρ,ϑ-system, one obtains the expression:

$$\frac{\left(x'-x^P\right)}{4\pi R^3}du_1du_2 = \frac{1}{4\pi\rho}\left(\frac{A_1(\vartheta)}{A^3(\vartheta)}+O(\rho)\right)d\rho d\vartheta \tag{30}$$

The extraction of the singularity in (30) according to (9) produces the integrand:

$$\left[\frac{1}{4\pi}\frac{A_1(\vartheta)}{\rho A^3(\vartheta)}-\frac{\left(x'-x^P\right)}{R^3}\frac{e^{\beta'r}}{4\pi}\rho\cos(\beta'r)\right]-\frac{1}{4\pi}\frac{A_1(\vartheta)}{\rho A^3(\vartheta)} \tag{31}$$

As the limit $O(\rho)/\rho \to O(1)$ in the first parenthesis in (31) exists, the singularity in the first term is lifted and the integrand is regular. The integration is then carried out e.g. by the method in section 3.1 in polar coordinates $\rho(\vartheta)$ and ϑ for all rectangles V_k:

$$\frac{1}{4\pi} \sum_{k=1}^{4} \int_{\vartheta_{il}}^{\vartheta_{iu}} \int_0^{\rho_k'(\vartheta)} \left[\frac{1}{\rho} \frac{A_1(\vartheta)}{A^3(\vartheta)} \right.$$

$$\left. - \frac{\left(x'(\rho,\vartheta)-x^P\right)}{R^3(\rho,\vartheta)} e^{\beta''r(\rho,\vartheta)} \rho \cos\left(\beta'R(\rho,\vartheta)\right) \right] d\rho d\vartheta \quad (32)$$

For the evaluation of the extracted term in (31), the Cauchy-limit is computed:

$$-\frac{1}{4\pi} \lim_{\rho_\varepsilon(\vartheta)\to 0} \sum_{k=1}^{4} \int_{\vartheta_{il}}^{\vartheta_{iu}} \int_{\rho_\varepsilon(\vartheta)}^{\rho_k'(\vartheta)} \frac{A_1(\vartheta)}{\rho A^3(\vartheta)} d\rho d\vartheta$$

$$= -\frac{1}{4\pi} \lim_{\rho_\varepsilon(\vartheta)\to 0} \sum_{k=1}^{4} \int_{\vartheta_{il}}^{\vartheta_{iu}} \frac{A_1(\vartheta)}{A^3(\vartheta)} \ln\left(\frac{\rho_k'(\vartheta)}{\rho_\varepsilon(\vartheta)}\right) d\vartheta \quad (33)$$

Now, introduce an ε vicinity using polar coordinates:

$$R_\varepsilon^2 = \varepsilon^2 = \left(x'-x^P\right)^2 + \left(y'-y^P\right)^2 + \left(z'-z^P\right)^2$$

$$= \rho_\varepsilon^2(\vartheta) A^2(\vartheta) + O(\rho_\varepsilon^3(\vartheta)) \quad (34)$$

This is then:

$$\rho_\varepsilon(\vartheta) = \frac{\varepsilon}{A(\vartheta)} \sqrt{1 - \frac{O(\rho_\varepsilon^3(\vartheta))}{\varepsilon^2}} = \frac{\varepsilon}{A(\vartheta)} - O(\varepsilon^2) \quad (35)$$

(35) in (33), one obtains

$$-\frac{1}{4\pi} \lim_{\varepsilon\to 0} \sum_{k=1}^{4} \int_{\vartheta_{il}}^{\vartheta_{iu}} \frac{A_1(\vartheta)}{A^3(\vartheta)} \left\{ \ln\left(\rho_k'(\vartheta)\right) - \ln\left(\frac{\varepsilon}{A(\vartheta)} - O(\varepsilon^2)\right) \right\} d\vartheta$$

$$= -\frac{1}{4\pi} \sum_{k=1}^{4} \int_{\vartheta_{il}}^{\vartheta_{iu}} \frac{A_1(\vartheta)}{A^3(\vartheta)} \ln\left(\rho_k'(\vartheta)A(\vartheta)\right) d\vartheta \quad (36)$$
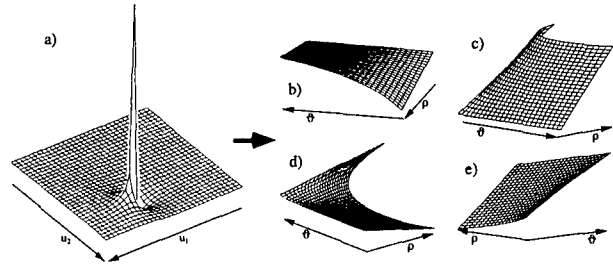
with (see also [GC87], [GG90], [HRHR97], [PG89])

$$\frac{1}{4\pi} \lim_{\varepsilon\to 0} \left[\sum_{k=1}^{4} \int_{\vartheta_{il}}^{\vartheta_{iu}} \frac{A_1(\vartheta)}{A^3(\vartheta)} d\vartheta \right] (\ln\varepsilon) = 0 \quad (37)$$

The expression in brackets vanishes when carrying out the integration and summation before taking the limit. Then the limit does not need to be carried out anymore. The strongly singular part in (9) caused by the derivative of the Green's function, is now readily treated by (31), (32), and (36).

Consider the integrand in (32). In Fig. 6a), the integrand is shown in the u_1,u_2-system. It is then transformed into the sub-integrands as in Fig. 6b) to e). The sub-integrands are formed by the sub-division process in Fig. 2. The integration domains are:

- Fig. 6b): $4,02 \le \vartheta < 5,18$ and $\rho(\vartheta) = -1,5/\sin(\vartheta)$,
- Fig. 6c): $-1,1 \le \vartheta < 0,59$ and $\rho(\vartheta) = 0,75/\cos(\vartheta)$,
- Fig. 6d) $0,59 \le \vartheta < 2,76$ and $\rho(\vartheta) = 0,5/\sin(\vartheta)$.
- Fig. 6e): $2,76 \le \vartheta < 4,02$ and $\rho(\vartheta) = -1,25/\cos(\vartheta)$.

Figure 6   Transform of the strongly singular integrand into regular sub-domains using a transform to polar coordinates and a singularity extraction. Integrands in sub-domains are normalized.

3.3.2   Domain transform and extraction of singularity

The new method combines the domain transform and the extraction of singularity in a convenient way. Analogous to 3.3.1, the strongly singular part (9) due to the derivative of the Green's function is treated. The order of the singularity is reduced by one by virtue of the integration weight $du_1 du_2 = 2A^D ds_1 ds_2 = A^D(t_1+1)/4\, dt_1 dt_2$ in (19) (see 3.2.2). This weight is formed by the transform of the differentials from the u_1,u_2-system into the t_1,t_2-system. (15) to (18) show the transform for $u_{1k}(t_1,t_2)$ and $u_{2k}(t_1,t_2)$. $k = 1...4$ are the number of the triangle in Fig. 4. One obtains for (9) with (19) for the x-component the weakly singular integrand:

$$\sum_{k=1}^{4} \frac{\left(x_k'(t_1,t_2)-x^P\right)}{R_k^3(t_1,t_2)} \frac{e^{\beta''R_k(t_1,t_2)}}{4\pi} \left[-\cos\left(\beta'R_k(t_1,t_2)\right)\right] \frac{A^{D_k}(t_1+1)}{4} \quad (38)$$

In (38), the singular point P is mapped onto the edge $t_1 = -1$. In contrast to 3.2.3 and 3.3.1, the distance factor is not expressed in the u_1,u_2-system around the point P, but rather in the t_1,t_2-system along the edge $t_1 = -1$. Using a series expansion, the extracted term is analytically integrable according to t_1. For the x-component (the y- and z-components are analogous) one obtains:

$$\left(x_k'-x^P\right) = \left.\frac{\partial x_k'}{\partial t_1}\right|_{t_1,-1} (t_1+1) + O\left((t_1+1)^2\right) \quad (39)$$

$$R_k^2(t_1,t_2) = (t_1+1)^2 f_k^2(t_2) + O\left((t_1+1)^3\right) \quad (40)$$

with

$$f_k(t_2) = \sqrt{\left.\left(\frac{\partial x_k'}{\partial t_1}\right)^2\right|_{t_1,-1} + \left.\left(\frac{\partial y_k'}{\partial t_1}\right)^2\right|_{t_1,-1} + \left.\left(\frac{\partial z_k'}{\partial t_1}\right)^2\right|_{t_1,-1}} \quad (41)$$

The term needed for the extraction of the singularity is given by (39) - (41). With (38), they yield:

$$\frac{1}{16\pi}\sum_{k=1}^{4}A^{D_k}\left[\left.\left[\frac{1}{(t_1+1)f_k^3(t_2)}\frac{\partial x_k'(t_1,t_2)}{\partial t_1}\right]\right|_{t_1=-1}\right.$$

$$\left.-\frac{x_k'(t_1,t_2)-x^P}{R_k^3(t_1,t_2)}e^{\beta''R_k(t_1,t_2)}\cos\left(\beta'R_k(t_1,t_2)\right)(t_1+1)\right]\quad(42)$$

$$-\frac{1}{16\pi}\sum_{k=1}^{4}A^{D_k}\left.\frac{1}{(t_1+1)f_k^3(t_2)}\frac{\partial x_k'(t_1,t_2)}{\partial t_1}\right|_{t_1=-1}$$

The terms in the brackets are regular

$$\frac{1}{16\pi}\sum_{k=1}^{4}A^{D_k}\int_{t_1=-1}^{t_1=+1}\int_{t_2=-1}^{t_2=+1}\left[\left.\left[\frac{1}{(t_1+1)f_k^3(t_2)}\frac{\partial x_k'(t_1,t_2)}{\partial t_1}\right]\right|_{t_1=-1}\right.$$

$$\left.-\frac{x_k'(t_1,t_2)-x^P}{R_k^3(t_1,t_2)}e^{\beta''R_k(t_1,t_2)}\cos\left(\beta'R_k(t_1,t_2)\right)(t_1+1)\right]dt_1dt_2\quad(43)$$

The integration is carried out using the method in 3.1.

For the second term in (42), the Cauchy limit is formed with the substitution $t = t_1 + 1$:

$$-\frac{1}{16\pi}\sum_{k=1}^{4}A^{D_k}\int_{t_1=-1}^{t_1=+1}\int_{t_\varepsilon}^{t_\varepsilon=2}\left.\frac{1}{tf_k^3(t_2)}\frac{\partial x_k'(t_1,t_2)}{\partial t_1}\right|_{t_1=-1}dtdt_2\quad(44)$$

For $t_\varepsilon \to 0$, one introduces an ε-vicinity as in (40)

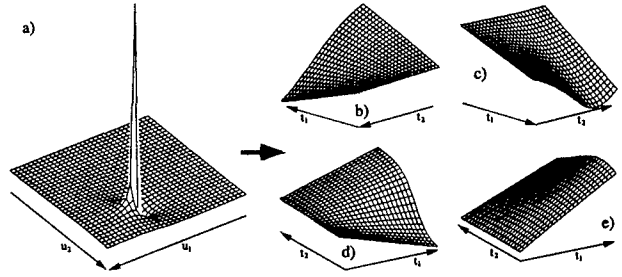$$R_\varepsilon^2 = \varepsilon^2 = t_\varepsilon^2 f^2(t_2) + O(t_\varepsilon^3),\quad(45)$$

one then obtains from (44)

$$-\frac{1}{16\pi}\lim_{\varepsilon\to0}\sum_{k=1}^{4}A^{D_k}$$

$$\int_{t_1=-1}^{t_1=+1}\left.\frac{1}{f_k^3(t_2)}\frac{\partial x_k'(t_1,t_2)}{\partial t_1}\right|_{t_1=-1}\left(\ln\left(2f_k(t_2)\right)-\ln\varepsilon\right)dt_2\quad(46)$$

$$= -\frac{1}{16\pi}\sum_{k=1}^{4}A^{D_k}\int_{t_1=-1}^{t_1=+1}\left.\frac{1}{f_k^3(t_2)}\frac{\partial x_k'(t_1,t_2)}{\partial t_1}\right|_{t_1=-1}\ln\left(2f_k(t_2)\right)dt_2$$

with (see (37))

$$\lim_{\varepsilon\to0}\sum_{k=1}^{4}A^{D_k}\int_{t_1=-1}^{t_1=+1}\left.\frac{1}{f_k^3(t_2)}\frac{\partial x_k'(t_1,t_2)}{\partial t_1}\right|_{t_1=-1}dt_2\ln(\varepsilon)=0\quad(47)$$
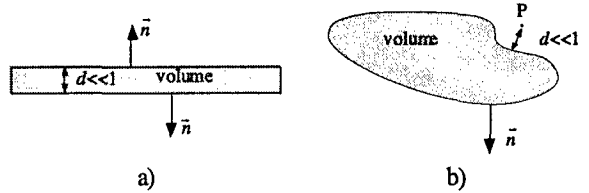
The integration method is now visualized by the example of the integrand in (43) as derived from (9). The strongly singular integrand in the u_1,u_2-system is in Fig. 7a). The integrands after transform and extraction are shown in the t_1,t_2-system in Fig. 7b) to 7e). The strongly singular part in (9) is transformed into a very smoothly varying function. Hence, the integration is carried out accurately with only a few nodes ensureing a fast computation.

Figure 7 Transform of the strongly singular integrand into regular sub-domains using a domain transform and a singularity extraction. Integrands in sub-domains are normalized.

3.4 Nearly Singular Integration

The integrands in Method of Moment computations are nearly singular when structures with a small thickness are to be computed, or if fields very close to a surface must be evaluated. In the first case, the problem is noticeable when setting up the matrix, in the second case when computing the fields after the surface currents have been computed. Figures 8a) and 8b) show the two cases. In Fig. 8a), the distance between two disrcrete surface elements is very small compared to the dimensions of the elements. In Fig. 8b), the distance d of an observation point P to the surface is smaller than the geometrical dimensions of the discretization elements.

Figure 8 Cases when nearly singular integrals are encountered.

The straight-forward method to evaluate nearly singular integrals is to increase the number of nodes within the numerical quadrature method. In this case, the number of nodes increases very quickly when the distance d is reduced.

A second method is to solve the nearly singular integrals by subdividing the surface elements in smaller elements, and to continue the subdivision process until convergence is achieved. This ensures that the number of nodes is increased in the vicinity of the observation point. The subdivision process is numerically expensive and is inefficient for very small distances d. Furthermore, the accuracy of a Gauss-Legendre quadrature depends on the number of nodes: The integration using 5 nodes of an element that has been

subdivided into two elements allows a correct integration of a polynomial of the 9th order on each subelement. Without the subdivision process, a polynomial of the 19th order could be integrated.

The efficient approach in [Tel87] und [Hay92] is to transform the surface variables u_1, u_2 in such a way that the resulting Jacobian lifts the nearly-singularity. This is to say that the Jacobian should approach the distance d at the critical point [Tel87], [Hay92]. The transform also concentrates the nodes around the location of the near-singularity which leads to a better integration.

4.   Example Integrals

The previously presented methods for integrations in Method of Moments computations are now applied to an analytical problem. The integrals in Table 3 are derived from the integrals in Table 1 to yield the analytically integrable functionals (48) and (49). The geometry for the verification is a quadratic surface element that is centered at the origin as in Fig. 1. Each side has a length of 2 m at a wavelength of 20 m. Hence, the length of each side is $\lambda/10$. The observation point P is located at $x = 0.25$ m, $y = 0.5$ m and a variable height z. The source point is located at $z = 0$.
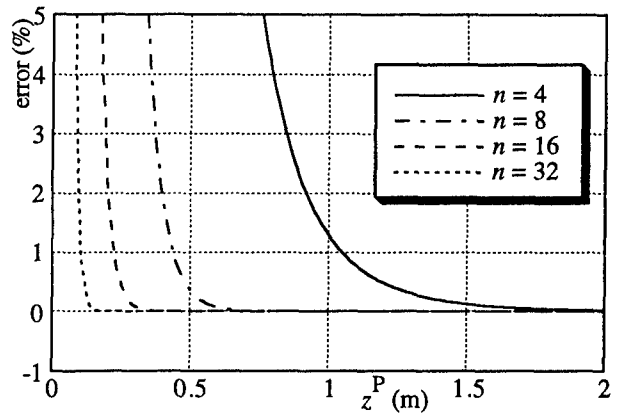
Table 3   Example integrals for the verification of the integration methods.

weakly singular kernel	$\dfrac{1}{4\pi}\displaystyle\iint_{S'} \dfrac{\vec{r}' - \vec{r}^{P}}{\left|\vec{r}' - \vec{r}^{P}\right|^{2}} dS'$ (48)	
$R \to 0$	weakly singular	$\to$ 4.2

strongly singular kernel	$\dfrac{1}{4\pi}\displaystyle\iint_{S'} \dfrac{\vec{r}' - \vec{r}^{P}}{\left|\vec{r}' - \vec{r}^{P}\right|^{3}} dS'$ (49)	
$\left.\begin{array}{l} R > d \\ R < d \end{array}\right\}$	regular	$\to$ 4.1
$R \to 0$	strongly singular	$\to$ 4.3
$R < d$	nearly singular	$\to$ 4.4

The integral is solved analytically and numerically, the following error evaluates the quality of the method:

$$\text{error in } \% = \frac{\left|\text{analytical - numerical}\right|}{\left|\text{analytical}\right|} \cdot 100 \qquad (50)$$

Note that it is only possible to analytically solve the integrations in Table 3 for planar geometries, not for arbitrary ones.

Figure 9   Regular integrand. Error for various locations z of observation point and number of nodes.
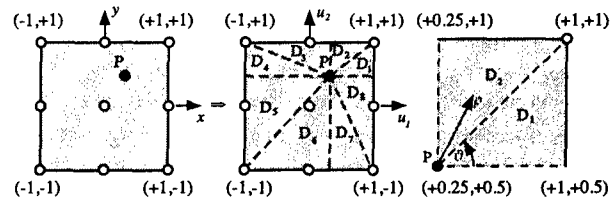
4.1   Regular Integrals

The observation point P is located at distances from $z^{P} = 0.01$ m to $z^{P} = 2$ m from the surface element. Consequently, the kernel varies from nearly singular $R < d$ to regular $R > d$. An integration using the Gauss-Legendre in 3.1 with $n \times n$ nodes yields the error in Fig. 9. For large distances from the surface to the observation point P, very few nodes are sufficient for a very low error. The error increases with decreasing distance z but can be decreased by using more nodes. The method fails for very small distances $z < 0.25$ m.

4.2   Weakly Singular Integrals

The observation point is located at $z^{P} = 0$ on the surface of the element.

4.2.1   Transform to Polar Coordinates

The integration of (48) is carried out by subdividing the surface element into four sub-elements, shown in Fig. 10 (middle) as dashed lines. The surface integration on each quadrangle composed of two triangles D_{k} and D_{k+1} with $k = 1...8$ (Fig. 10 rightmost) again involves $n \times n$ nodes. $n/2$-nodes are used for the ϑ-integration per triangle D_{k}, the integration according ρ is then carried out using n nodes.

Figure 10   Surface element ($z = 0$) and representation with normalized, local coordinates. The rectangle is subdivided into four quadrangles composed of two triangles each.

The integration of (48) is itemized in Table 4. Convergence is fast with increasing number of nodes to the correct value. For $n > 32$, no improvements are observed, the result is stable with an increasing number of nodes.

Table 4 Weakly singular integration of (48) with transform into polar coordinates. Analytical result is -0.0579393378.

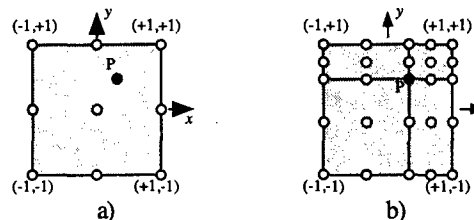| n	result	error (%)
2	-0.0519166274	10.39
4	-0.0570911480	$14.64 \cdot 10^{-1}$
6	-0.0578289883	$19.05 \cdot 10^{-2}$
8	-0.0579257050	$23.53 \cdot 10^{-3}$
16	-0.0579393352	$45.73 \cdot 10^{-7}$
32	-0.0579393378	$71.31 \cdot 10^{-10}$
64	-0.0579393378	$26.96 \cdot 10^{-10}$

4.2.2 Domain Transform

The surface element is sub-divided into four triangles that are in turn mapped to quadrangles. Again, the integration involves $n \times n$-nodes corresponding to the number of nodes of the previous example. Table 5 shows the results for the method. Again, convergence to the correct value is observed with a stable result beyond $n = 32$ nodes.

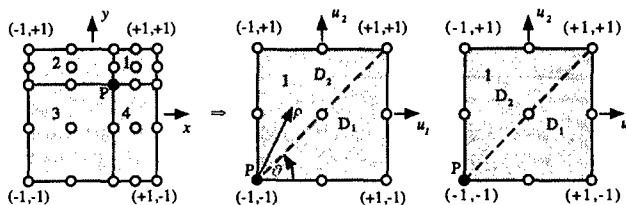**Table 5** Weakly singular integration of (48) with domain transform. Analytical result is -0.0579393378.

n	result	error (%)
2	-0.0360523044	37.78
4	-0.0549348239	$51.86 \cdot 10^{-1}$
6	-0.0578618391	$13.38 \cdot 10^{-2}$
8	-0.0579760027	$63.28 \cdot 10^{-3}$
16	-0.0579393184	$33.55 \cdot 10^{-6}$
32	-0.5793933785	$22.88 \cdot 10^{-10}$
64	-0.0579393378	$14.28 \cdot 10^{-10}$

4.3 Strongly Singular Integration

The strongly singular integration (49) with the observation point $P(x = 0,25 \text{ m}, y = 0,5 \text{ m}, z = 0)$ is carried out according to the Cauchy singular integral. The integration domain is subdivided into four sub-domains as in Fig. 11. This permits the evaluation of the accuracy of the surface integral and the line integral. Fig 11a) shows a discretization into only one surface element. Fig. 11b) discretizes the geometry into four elements, the observation point is then on the corner common to each discretization element. For

Figure 11 Two discretizations of the geometry in Fig. 1 for $P(x = 0.25 \text{ m}, y = 0.5 \text{ m}, z = 0)$.

Figure 12 Surface element $(z = 0)$ and representation with transform to polar coordinates (middle) and domain transform (rightmost). Polar coordinates: The rectangle is subdivided into four quadrangles. Domain transform: The rectangle is subdivided into four quadrangles composed of two triangles each. Only element 1 (upper right corner) is shown.

the discretization in Fig. 11a) the surface integral in (49) vanishes (see 3.3), the integration is completely determined by the line integral. In Fig. 11b) both terms contribute to the result.

The transforms in turn are sketched in Fig. 12.

4.3.1 Transform to Polar Coordinates and Extraction of Singularity

[GG90] evaluates the integral for many combinations of observation points and surface elements. These cases have been verified with the present method. The transform is shown in Fig. 12 (middle).

For a discretization into one element (cf. Fig. 11a), the results are summarized in Table 6. A good convergence is observed for an increasing number of nodes. For $n = 6$, an error of almost 0.05 % is achieved. The method remains stable for a larger number of nodes.

The integration according to Fig. 11b) maps the observation point to $u_1 = -1$, $u_2 = -1$ in local coordinates (Fig. 12 middle). For each triangle, $n \times n$ nodes are used, the line integral uses again n nodes. Table 7 shows the results of the integration. More nodes are needed for the same accuracy compared to a discretization into one element only.

Table 6   Strongly singular integration of (49) after transform to polar coordinates according to Fig. 10 and 11a). Analytical result is -0.052741730991244.

n	surface integral	line integral	error (%)
2	0	-0.0471475986	10.61
4	0	-0.0524191674	$61.16 \cdot 10^{-2}$
6	0	-0.0527116953	$56.95 \cdot 10^{-3}$
8	0	-0.0527389852	$52.06 \cdot 10^{-4}$
16	0	-0.0527417307	$49.36 \cdot 10^{-8}$
32	0	-0.0527417310	$54.90 \cdot 10^{-10}$
64	0	-0.0527417310	$18.89 \cdot 10^{-10}$

Table 7   Strongly singular integration of (49) after transform to polar coordinates according to Fig. 10 and 12. Analytical result is -0.052741730991244.

n	surface integral	line integral	error (%)
2	0.2416862365	-0.1793554832	$21.82 \cdot 10^{+1}$
4	0.1785239348	-0.2481406072	32
6	0.1849263635	-0.2398825203	$41.99 \cdot 10^{-1}$
8	0.1868837023	-0.2388539817	$14.63 \cdot 10^{-1}$
16	0.1864218113	-0.2391635614	$36.29 \cdot 10^{-6}$
32	0.1864218178	-0.2391635488	$12.23 \cdot 10^{-9}$
64	0.1864218178	-0.2391635488	$19.75 \cdot 10^{-10}$

Table 8   Strongly singular integration of (49) by domain transform according to Fig. 11a). Analytical result is -0.052741730991244.

n	surface integral	line integral	error (%)
2	0	-0.0883362945	67.49
4	0	-0.0615749331	16.75
6	0	-0.0529196853	$33.74 \cdot 10^{-2}$
8	0	-0.0525051309	$44.86 \cdot 10^{-2}$
16	0	-0.0527419384	$39.33 \cdot 10^{-5}$
32	0	-0.0527417310	$91.62 \cdot 10^{-11}$
64	0	-0.0527417310	$22.17 \cdot 10^{-10}$

Table 9   Strongly singular integration of (49) by domain transform according to Fig. 12. Analytical result is -0.052741730991244.

n	surface integral	line integral	error (%)
2	0.2330166165	-0.1652108191	$22.86 \cdot 10^{+1}$
4	0.1880115487	-0.2448561289	$77.79 \cdot 10^{-1}$
6	0.1809303725	-0.2427592011	17.23
8	0.1869992436	-0.2386698415	$20.31 \cdot 10^{-1}$
16	0.1864232112	-0.2391626624	$43.23 \cdot 10^{-4}$
32	0.1864218178	-0.2391635488	$19.17 \cdot 10^{-9}$
64	0.1864218178	-0.2391635488	$39.71 \cdot 10^{-10}$

4.3.2   Domain Transform and Extraction of Singularity

The integration with domain transform and subsequent extraction of the singularity yields the results in Table 8. The integration shows stable results for an increasing number of nodes. An accuracy of better than 0.01 % is reached for 16 nodes.

A discretization according to Fig. 11b) results in a subdivision as shown in Fig. 12 for the element 1. The singularity is located at $u_1 = -1$, $u_2 = -1$ for each triangle. The integration is carried out according to 3.3.2, $n \times n$ nodes are used. Table 9 shows the results for both surface and line integrals. A stable convergence is achieved, an error better than 0.01 % is obtained for $n = 16$.
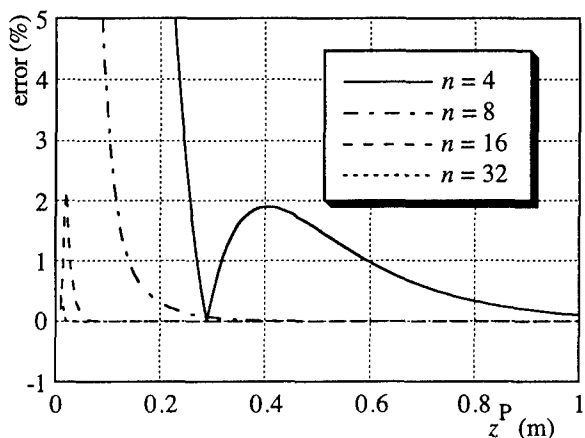
The integrations in 3.3.1 and 3.3.2 yield both results within the same range of accuracy. For the result shown, the method in 3.3.2 (viz. the domain transform and subsequent extraction of singularity) results in smaller errors for only few nodes.

4.4   Nearly singular integrals

As seen in 3.1, the integration using a Gauss-Legendre quadrature when the observation point is close to a surface (see Fig. 1) yields only slowly converging results. A large number of nodes is required. Even for $n = 32$, the error reaches 3000 % for an observation point located at $z^r = 0.01$ m. The method in [Tel87], [Hay92] allows a fast integration with a high level of accuracy.

Fig. 13 shows the error obtained with the method in 3.4 for an increasing number of nodes. The shortest distance between an observation and a source point is $z^r = 0.01$ m. The largest error is for $n = 16$ at a distance of $z^r = 0.02$ m and evaluates to 2.1631 %. For $n = 32$, this error is reduced to 0.2106 %.

Figure 14 shows a comparison between the methods in 3.1 and 3.4 for the same number $n = 4$ and $n = 32$. It is clear from this picture that the integration according 3.4 yields much better results for nearly singular integrals.

Figure 13 Nearly singular integrand. Error curves for an increasing number of nodes with observation point at various distances to the surface element.

Figure 14 Nearly singular integrand. Error curves for the methods in 4.1 and 4.4 and an increasing number of nodes with observation point at various distances to the surface element.
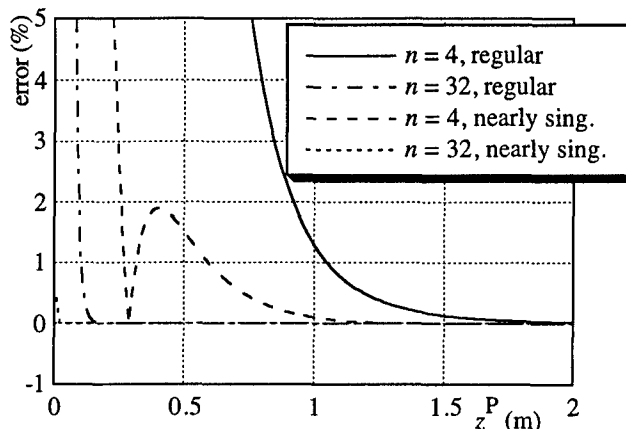
5.   Conclusions

By properly identifying the orders of the singularity with the reaction integrals of the Method of Moments formulation, appropriate integration methods are found to be applicable for each of the integrals. Regular integrals are solved by a Gauss-Legendre quadrature. Weakly singular integrals necessitate a regularization, and are then integrated numerically. Strongly singular integrals are regularized by a two stage process and integrated both analytically and numerically. The correct method ensures for each kernel a fast and stable convergence to the correct values.

The methods are general enough to be used as methods for surface integrals with various degrees of singularity. The methods are not restricted to Method of Moments formulations in Computational Electromagnetics.

BIBLIOGRAPHY

[Abr70]   M. Abramowitz, I.A. Stegun, *Handbook of Mathematical Functions*, Dover Publications, New York, 1970.

[Dom93] J. Dominguez, *Boundary Elements in Dynamics*, Computational Mechanics Publications, Southhampton, Co-published with Elsevier Applied Science, London, 1993.

[Duf82]   "Quadrature over a Pyramid or Cube of Integrands with a singularity at the Vertex", *SIAM J. Numer. Anal.*, Vol. 19, No 6, Dec. 1982.

[GC87]   M. Guiggiani, P. Casalini, "Direct Computation of Cauchy Principal Value Integrals in Advanced Boundary Elements", *International Journal for Numerical Methods in Engineering*, Vol. 24, pp. 1711-1720, 1987.

[GG90]   M. Guiggiani, A. Gigante, "A General Algorithm for Multidimensional Cauchy Principal Value Integrals in the Boundary Element Method", *Transactions of the ASME*, Vol. 57, pp. 906-915, December 1990.

[HvHW00]   A. Herschlein, J. v. Hagen, W. Wiesbeck, "Electromagnetic scattering by Arbitrary Surfaces Modelled by Linear Triangles and Biquadratic Quadrangles", *IEEE Symposium on Antennas and Propagation 2000*, Salt Lake City, UT, USA, 2000, Vol. 4, pp. 2290-2293.

[Hay92]   K. Hayami, *A Projection Transformation Method for Nearly Singular Surface Boundary Element Integrals*, Springer-Verlag, 1992.

[HRHR97]   C.J. Huber, W. Rieger, M. Haas, W.M. Rucker, "The numerical treatment of singular integrals in boundary element calculations", *ACES Journal*, vol. 12, nu. 2, pp. 121-126, 1997.

[PG89]   P. Parreira, M. Guiggiani, "On the Implementation of the Galerkin Approach in the Boundary Element Method", *Computers & Structures*, Vol. 33, pp. 269-279, 1989.

[PM73]   A. J. Poggio, E. K. Miller, "Integral Equation Solutions of Three-Dimensional Scattering Problems" in *Computer Techniques for Electromagnetics*, Volume 7, edited by R. Mittra, Pergamon Press, New-York, NY, USA, 1973.

[SC95]   J.M. Song, W.C. Chew, "Moment Method Solutions using Parametric Geometry", *Journal of Electromagnetic Waves and Appl.*, Vol. 9, No. 1/2, pp. 71-83, January-February, 1995.

[Sch93]   H.R. Schwarz, *Numerische Mathematik*, B.G. Teubner, Stuttgart, 1993.

[Tel87]   J.C.F. Telles, "A self-adaptive coordinate Transformation for efficient numerical Evaluation of general Boundary Element Integrals", *International Journal for Numerical Methods in Engineering*, Vol. 24, pp. 959-973, 1987.